


## Article

# Design and Optimization of High Ground Clearance Self-Propelled Sprayer Chassis Frame

Liquan Lu <sup>1</sup>, Bin Liu <sup>2</sup>, Enrong Mao <sup>3</sup>, Zhenghe Song <sup>3</sup>, Jun Chen <sup>1</sup> and Yu Chen <sup>1,\*</sup> <sup>1</sup> College of Mechanical and Electronic Engineering, Northwest A&F University, Xianyang 712100, China<sup>2</sup> Beijing Electric Vehicle Co., Ltd., Beijing 102606, China<sup>3</sup> Beijing Key Laboratory of Optimized Design for Modern Agricultural Equipment, China Agricultural University, Beijing 100083, China

\* Correspondence: jdx73@nwfau.edu.cn

**Abstract:** As an important machine for agricultural application, the upland gap self-propelled sprayer is environmental friendly and operates efficiently. In this paper, the chassis frame, which is one of the important components of the sprayer, is studied and a disconnected longitudinal beam frame with an X-shaped reinforcement beam was designed. The static mechanical properties of the frame under bending, torsion, emergency braking and emergency turning conditions are analyzed by a finite element method, and the optimization idea was proposed. On this basis, the topology optimization method was applied to optimize the crossbeam and the reinforcement beam positions, resulting in a 2.2% reduction in the overall mass of the frame, a 19.4% reduction in the maximum deformation while maintaining a small change in the maximum stress in the bending condition, and a 4.1% and 15.1% reduction in the maximum deformation and maximum stress of the frame in the torsion condition, respectively. The frame section width and thickness parameters were optimized by multi-objective driven optimization. The results showed that the frame mass and maximum stress were reduced by 6.8% and 1.9%, respectively, in the bending condition at the cost of a slight increase in frame deformation.

**Keywords:** self-propelled sprayer; chassis frame; finite element analysis; topology optimization



**Citation:** Lu, L.; Liu, B.; Mao, E.; Song, Z.; Chen, J.; Chen, Y. Design and Optimization of High Ground Clearance Self-Propelled Sprayer Chassis Frame. *Agriculture* **2023**, *13*, 233. <https://doi.org/10.3390/agriculture13020233>

Academic Editor: Xiuliang Jin

Received: 4 January 2023

Revised: 13 January 2023

Accepted: 17 January 2023

Published: 18 January 2023



**Copyright:** © 2023 by the authors. Licensee MDPI, Basel, Switzerland. This article is an open access article distributed under the terms and conditions of the Creative Commons Attribution (CC BY) license (<https://creativecommons.org/licenses/by/4.0/>).

## 1. Introduction

Application technology is a key technology for high and stable agricultural production [1], and the backwardness of application technology and plant protection machinery technology in China not only seriously weakens the resistance to pests and threatens food security, but also is harmful to the safety of the agricultural ecological environment and restricts the sustainable development of Chinese agriculture [2]. As an important machine for plant protection and medicine application [3–5], the high ground clearance self-propelled sprayer has the characteristics of easy mobility, wide spraying width, uniform spraying, high efficiency and wide application [6–8]. Therefore, to improve the operational performance of highland gap self-propelled sprayer is an important means to develop the application technology [9]. The chassis frame is an important part of the sprayer to connect and support other parts and ensure its normal operation. Compared with other vehicles, sprayers should ensure stable spraying performance and try to avoid the excessive shaking of the spray bar to improve the application quality [10–13], so the rigidity of the frame has high requirements. At the same time, the sprayer operates under complex conditions, mainly on the field road [14–16], and the frame is required to have a certain strength in order to safely cope with the dynamic impact load from the road. Therefore, it is essential to further design and optimize the frame structure of the sprayer chassis.

At present, research on the chassis of sprayers mainly focuses on the drive, steering, suspension system and frame [17–20]. Xue X B designed a hedge shaped sprayer frame, carried out finite element analysis and optimized the structure of the frame to make the

stress distribution more uniform [21]. Chen Y et al. designed a large upland gap self-propelled sprayer chassis, analyzed the structural composition and working principle of the drive system, suspension system and frame, and conducted finite element analysis of the frame under different working conditions of the sprayer [22]. Wu B designed a hydraulic chassis frame for a self-propelled paddy spraying machine, and optimized the frame structure with the goal of light weight while conducting static and modal analysis [23]. Hong C et al. investigated the static performance of the frame of highland gap sprayers at ultimate torsion and full load by finite element simulation tests, and the mechanical performance of the frame under step excitation by multi-body dynamic simulation tests [24].

Structural design optimization can be classified into shape optimization, structural parameter optimization, dynamic performance optimization, etc., according to the type of design variables and optimization levels. Zheng X conducted a static and dynamic analysis of a large bus frame using the APDL language in ANSYS, optimized the important parameters of the model to achieve the purpose of light weight, and optimized the topology of the frame locally [25]. Liang J B and Liang J C used HyperWorks to optimize the topology of the engine mount of a heavy vehicle, and obtained the density contour distribution map of the mount by the variable density method, which led to a weight reduction of 15.96% for the cast mount and achieved good economic benefits [26]. Long K et al. established a finite element model of the tractor frame and performed a multi-case static analysis [27]. Based on the OptiStruct software, an engineering practical solution to the common problems of multi-case topology optimization was proposed to realize the optimized design of the tractor frame structure. Combined with the above research, if the optimization design theory is applied to the optimization of the frame layout and key dimensions of key components of the spraying machine, it will be beneficial to the frame to have better stiffness and strength performance while saving materials and achieving light weight, and improve the performance of the frame and the whole vehicle [28,29].

Combined with the above research progress, the research on the chassis frame of spraying machine is less, and most of them are aimed at design and calibration, but no deeper research and discussion on the structure has been conducted. In addition, if the optimization design theory is applied to the optimization of the spraying machine frame layout and key dimensions of key components, it will be more beneficial for the frame to have better stiffness and strength performance while saving materials and achieving light weight, and improving the performance of the frame and the whole vehicle. Therefore, this study proposes a new frame structure more suitable for sprayer spray discs, i.e., a frame with X-shaped reinforcement beams, and optimizes its structure by applying the optimization design theory, based on the layout form of sprayer and the characteristics of independent suspension chassis, and the main research contents include (1) design the overall structural plan of the frame and design calculations for key components, including the cross-sectional dimensions of the longitudinal and crossbeams of the frame; (2) static finite element analysis and calibration of the frame, and propose directions that can be optimized; (3) optimize the position of frame crossbeam and reinforcement beam by using topology optimization method; (4) optimize the frame section width and thickness parameters by multi-objective driven optimization, and compare and analyze the mechanical performance of the frame before and after optimization.

## 2. Materials and Methods

### 2.1. Equipment Structure Design

#### 2.1.1. General Layout of the Whole Vehicle

In the whole vehicle spring load mass, the cab, engine, tank and spray bar are the most important and largest quality components. Therefore, the overall arrangement of the sprayer mainly considers the location arrangement of the cab, engine, tank and spray bar, and the different arrangement methods will largely affect the structural form of the frame and the overall scheme. According to the current arrangement form of sprayers of major agricultural machinery companies at home and abroad and comparing their characteristics,

the overall arrangement form of sprayers with spray bar rear and engine center is finally chosen as shown in Figure 1. This arrangement can fully guarantee the driver's vision and reduce the influence of drug drift on the driver. In addition, the placement of the engine behind the medicine box also makes the installation of the drive unit and power distribution more convenient.

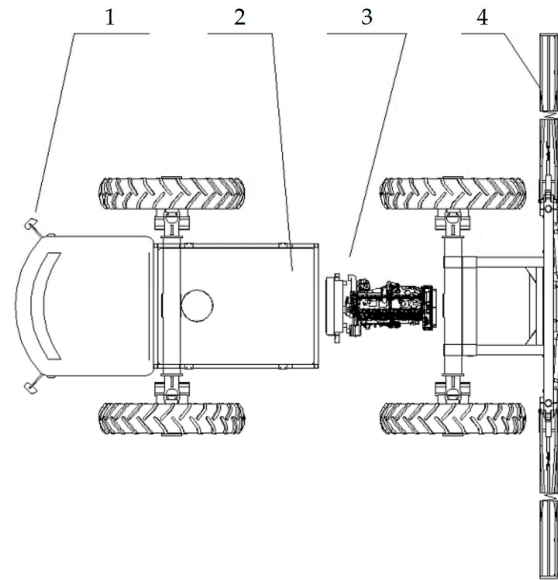


**Figure 1.** Overall arrangement plan of spraying machine. 1. Cockpit 2. Medicine cabinet 3. Engine 4. Spray bar.

#### 2.1.2. Frame Form Scheme Selection

The traditional frame is usually divided into side beam frame, X-shaped frame, perimeter frame, spine frame and integrated frame according to the different structural forms [30]. Agricultural vehicles are more diverse and special because of the diversity of their working forms and the complexity of their working environment. The high ground gap sprayer must not only consider the dynamic impact load on the field road during low-speed work, but also the smooth and stable driving during high-speed transportation. In the above-mentioned extreme working conditions, the frame will be subjected to various large bending moments and torques. This study intends to choose a disconnected longitudinal beam frame as shown in Figure 2. This frame can better withstand the bending and torque in the harsh environment and suitable for independent suspension type chassis. At the same time, in order to make the frame meet the higher stiffness requirements, the X-shaped frame with better torsional resistance is combined with the disconnected longitudinal beam frame, that is, the disconnected longitudinal beam frame with the X-shaped reinforcement beam.

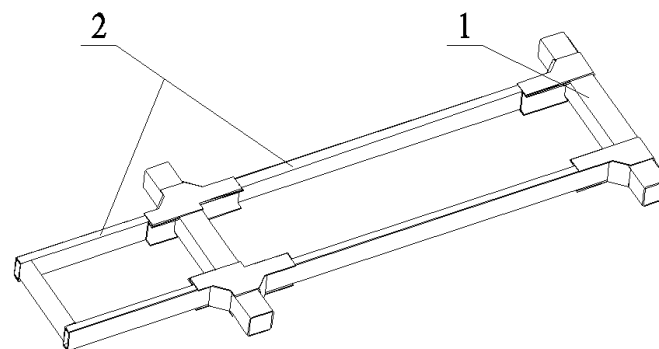


**Figure 2.** Disconnected longitudinal beam side beam type frame. 1. Axles (crossbeams) 2. Disconnected longitudinal beam.

### 2.1.3. Frame Outline Size Determination

The outline dimension of the frame mainly refers to the length and width of the main part of the frame. According to the frame form determined in the previous section, the frame length refers to the maximum value of the distance between the front cross member of the frame and the distal face of the rear axle. The total width refers to the maximum value of the distance between the left and right longitudinal beams of the main part of the frame. The specific dimensions depend on the shape dimensions and mounting dimensions of each assembly component according to the structural parameters of the whole vehicle, as shown in Table 1.

**Table 1.** Spraying machine structure parameters and installation dimensions.

Overall Vehicle Parameters	Value/mm
overall vehicle height	4000
overall vehicle length	7000
overall vehicle width	3600
standard ground gap	1900
track width	3000~3800 (adjustable)
wheelbase	3600
cab mounting base plate	1150 × 1540
medicine box mounting bracket	2100 × 1610
engine radiator assembly	1800 × 755
fuel tank mounting bracket	1000 × 400

The length of the frame is determined by the length of each assembly mounting bracket. The wider the width of the frame, the better the lateral stability of the vehicle and the stronger the torsional stiffness of the frame body. In the case that the width of the whole vehicle is determined, then the total length of the axle is determined, the wheelbase adjustment mechanism needs to be installed inside the axle. The longitudinal beam connection position needs to give way to the installation position of the wheelbase adjustment mechanism. Therefore, the main body of the frame needs to increase the width of the frame as much as possible under the condition of ensuring the adequate installation position of the wheelbase adjustment mechanism. The longitudinal beam at the front of the front axle has little influence on the torsional stiffness of the frame, so the overall width can be reduced appropriately to leave more space for the installation of the cab, ladder and other components. Therefore, through comprehensive consideration, the frame form of narrow front and wide rear is determined, with the width of the rear end of the frame body being 1070 mm and the front width being 940 mm. Based on the above analysis, the overall scheme of the finalized frame structure is shown in Figure 3.

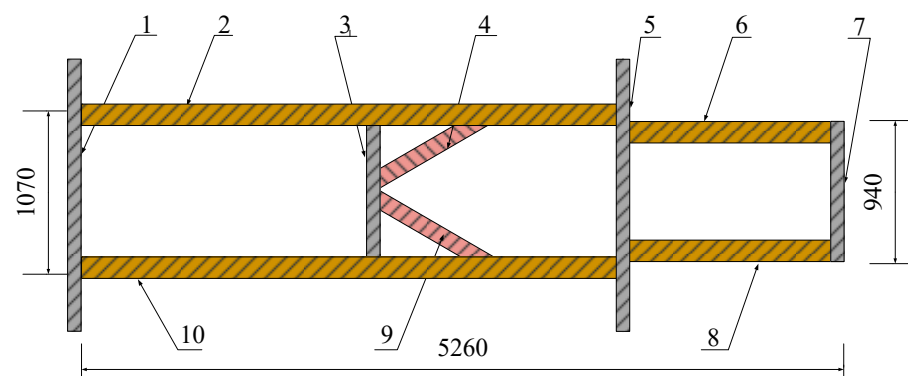


**Figure 3.** General scheme of frame structure.

In Figure 3, 1 and 5 are the axles simplified as crossbeams, with both ends protruding from the main frame body for mounting the wheelbase adjustment mechanism; 2 and 10



are the left and right longitudinal beams of the frame, which are the mounting benchmarks for most of the assembly components; 6 and 8 are the left and right longitudinal beams of the cab mounting area, which mainly bear the load of the cab area; 3 is the crossbeam in the middle of the frame; and 7 is the crossbeam in the front of the frame, mainly for strengthening the local strength and the overall frame 4 and 9 are X-type strengthening beams, the largest weight component pillbox assembly is installed in the middle and front of the frame, at this time, X-type strengthening beams can not only enhance the overall torsional rigidity of the frame, but also enhance the local strength of the pillbox installation area. Considering the wide application of Q345, its good mechanical properties are acceptable compared to the risk of less hardenability, so Q345A was initially selected as the raw material for the main beam of the chassis frame in this design.

2.2. Design of Key Equipment Components

2.2.1. Longitudinal Beam Design

The longitudinal beam of the frame is a stacked beam with a closed-ended section. Considering that the bending area of the longitudinal beam is a forbidden welding area, the wall thickness is determined conservatively for the first time as 10 mm, and the shape of the longitudinal beam section is shown in Figure 4a.

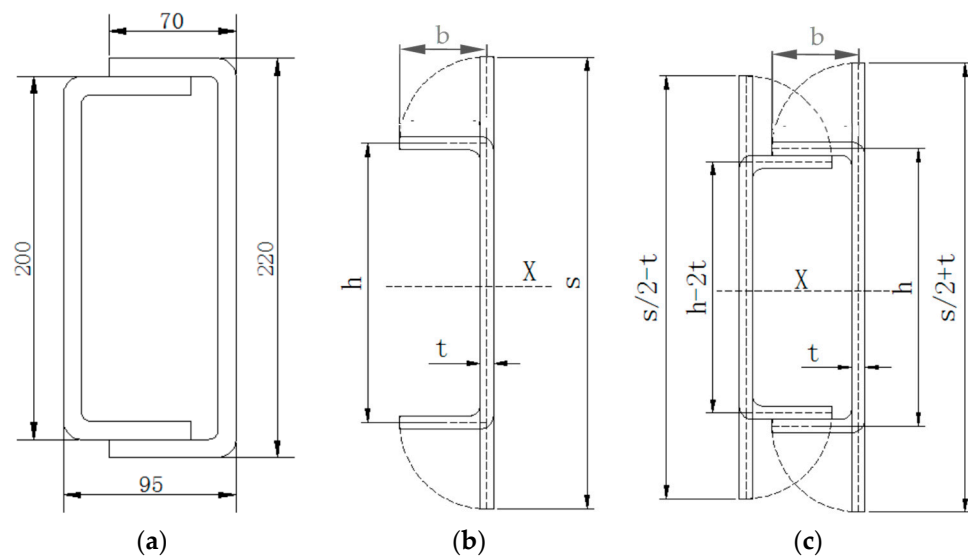


Figure 4. Longitudinal beam structure diagram. (a) Initial longitudinal beam section; (b) Slot cross-sectional drawing; (c) Stacked section diagram.

The stacked section is formed by superimposing two slotted section beams, so the bending resistance of the slotted section beam is considered first as shown in Figure 4b, and its unfolded width is

$$s = h + 2b \tag{1}$$

where  $s$  is the groove section unfolding length,  $h$  is the web height, and  $b$  is the airfoil length.

The introduction of aspect ratio  $\lambda \in (0, 1)$ , then

$$\lambda = \frac{h}{s} \tag{2}$$

The flexural capacity of a beam is usually measured by the flexural section coefficient, and the flexural capacity of a channel in the vertical direction is expressed by the flexural

coefficient  $W_X$ . Since the section is symmetrical with respect to the X-axis, the plane where the X-axis is located is the neutral plane, according to which we can get

$$W_X = \frac{th}{6}(h + 6b) \tag{3}$$

From Equations (1) and (2), we get

$$h = \lambda s, b = \frac{(1 - \lambda)s}{2} \tag{4}$$

Substituting into Equation (3) yields

$$W_X = \frac{\lambda(3 - 2\lambda)ts^2}{6} = F_{W_{X1}} \frac{ts^2}{6} \tag{5}$$

where, to facilitate the analysis of the effect of the value of aspect ratio  $\lambda$  on the value of  $W_X$ , let  $F_{W_{X1}} = 3\lambda - 2\lambda^2$ .

When  $\lambda$  changes from 0 to 1, the height-to-width ratio of the slotted section gradually increases, and the airfoil gradually becomes narrower, and the limit state is made by unfolding all of the two airfoils in pairs to make the web. The value of  $F_{W_{X1}}$  varies with  $\lambda$  as shown in Figure 5.

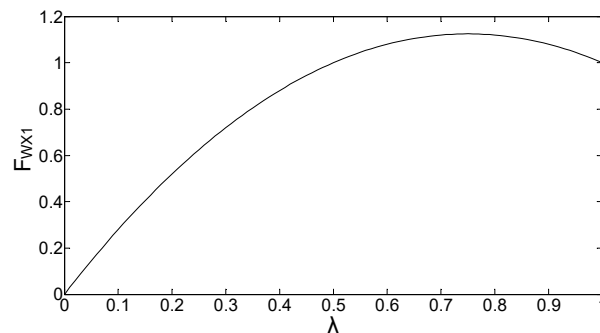


Figure 5. Diagram of the relationship between  $F_{W_{X1}}$  and  $\lambda$ .

As can be seen from Figure 5,  $F_{W_{X1}}$  takes the maximum value of 1.125 when  $\lambda = 0.75$ , indicating that the slotted section has the strongest bending resistance when the height-to-width ratio is 0.75. Based on the above results, the bending resistance of the stacked section is analyzed as shown in Figure 4c. The unfolded length of the stacked section is

$$s = 2h + 4b - 2t \tag{6}$$

Introducing the aspect ratio, with the outer slotted section set to  $\lambda_1$  and the inner slotted section to  $\lambda_2$ , then

$$\begin{cases} \lambda_1 = \frac{h}{s}, & \lambda_1 \in (\frac{t}{s}, 0.5 + \frac{t}{s}) \\ \lambda_2 = \frac{h-2t}{s}, & \lambda_2 \in (0, 0.5 - \frac{t}{s}) \end{cases} \tag{7}$$

where  $t$  is a constant of constant value.

Due to the symmetry of the section, the plane where the X-axis is located is neutral, and the bending section coefficient of the stacked section against the X-axis can be found as

$$W_X = \int y^2 dA / y_{\max} = \frac{th}{6}(h + 6b) + \frac{t(h - 2t)^2}{6} + tb(h - 2t) \tag{8}$$

The total cross-sectional length  $s$  is related to the cross-sectional thickness and cross-sectional area, with

$$\alpha = \frac{t}{s} \tag{9}$$

Substituting Equations (6), (7) and (9) into Equation (8) gives

$$W_X = \frac{s^3}{6}[-4\alpha\lambda_1^2 + (3\alpha + 8\alpha^2)\lambda_1] + K \tag{10}$$

where  $K$  is a constant related to  $\alpha$  and  $s$  only. Since  $\alpha$  is small, neglecting the higher order yields

$$W_X = \frac{s^3}{6}(-4\alpha\lambda_1^2 + 3\alpha\lambda_1) + K = (-4\lambda_1^2 + 3\lambda_1)\frac{\alpha s^3}{6} + K = F_{W_{X2}}\frac{\alpha s^3}{6} + K \tag{11}$$

where same as Equation (5), let  $F_{W_{X2}} = 3\lambda_1 - 4\lambda_1^2$ .

As  $\lambda_1$  changes from  $\frac{t}{s}$  to  $0.5 + \frac{t}{s}$ , the height-to-width ratio of the stacked section gradually increases and the airfoil gradually becomes narrower, with the limit state of four airfoils stacked to two ventral surfaces fitting together. The value of  $F_{W_{X2}}$  varies with  $\lambda_1$  as shown in Figure 6.

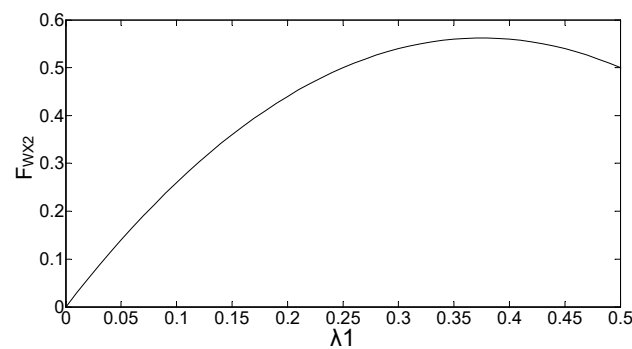


Figure 6. Diagram of the relationship between  $F_{W_{X2}}$  and  $\lambda_1$ .

As can be seen from Equation (10) and Figure 6, when  $\lambda_1 = 0.375$ ,  $F_{W_{X2}}$  takes the maximum value of 0.5625, which means that the bending resistance of the stacked section is the strongest when the height-to-width ratio of the outer slotted section is  $0.375 + \frac{t}{s}$ . At this time, the height-to-width ratio of the inner slotted section is  $0.375 - \frac{t}{s}$ .

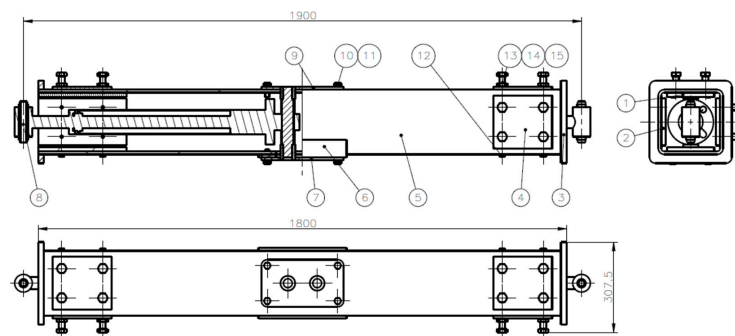
The cross-sectional dimensions of the beams depend not only on their mechanical properties requirements, but also on the specific installation and processing conditions, etc. In the overall scheme of the design, a disconnected longitudinal beam is used, and the vertical dimension of the longitudinal beam section is constrained by the outer dimensions of the crossbeam (axle), which need to be standard square steel dimensions, so the  $h$  cannot be fine-tuned. If the  $b$  is fine-tuned to better exploit the mechanical properties of the material in order to fit the theoretical calculation results, the relevant results after improvement are shown in Table 2.

Table 2. Calculation results of section size fine-tuning.

Cross-Sectional Parameters	b	s	$\lambda$	$\lambda_1$	$\lambda_2$	$W_X$
initial value	65 mm	660 mm	0.618/0.594	0.318	0.288	393,667 mm <sup>3</sup>
improvement value	60 mm	640 mm	0.636/0.613	0.328	0.297	373,667 mm <sup>3</sup>
range of change/%	-7.7	-3.0	2.9/3.2	3.1	3.1	-5.1

### 2.2.2. Crossbeam Design

In order to increase the chassis frame stiffness and strength, the upper and lower flanges and webs of the crossmember and longitudinal beam are all connected when connecting the crossmember and longitudinal beam. Considering the convenience of processing and assembly, the crossmembers are all selected from standard steel sections. In Figure 3, standard square steel is selected for the axles of 1 and 5, standard rectangular steel is selected for the crossmembers of 3 and 7 and standard channel steel is selected for the strengthening beams of 4 and 9. In this study, the front and rear axles are simplified as the crossbeams are connected with the frame as a whole, and also have the role of wheelbase adjustment. Figure 7 shows the assembly diagram of the designed axle.



**Figure 7.** Axle assembly diagram. 1, 2. sliding plate; 3. wheel edge limit plate; 4. thickening plate; 5. bridge shell; 6. strengthening plate; 7, 9. window cover plate; 8. wheel distance adjustment hydraulic cylinder; 10, 11. bolt lock washer; 12. bolt; 13, 14, 15. bolt nut lock washer.

In Figure 7, 5 is the axle housing, the standard square steel of  $220 \times 220 \times 10$  is selected, the type of hydraulic cylinder 8 is selected from the initial wheelbase adjustment range, and the overall length of the axle is 1800 mm according to the shape size and installation method of the hydraulic cylinder. The slide plate 2 is fixed directly to the inner wall of the axle housing by the bolt washer combination 12, and there are four blind holes on the slide plate 1. The bolt-locking washer combination 13~15 is inserted into the blind holes by the thickened plate 4 to press the slide plate 1 and the sliding square steel, which has the effect of locking after adjusting the wheelbase.

### 2.3. Frame Finite Element Modeling

The finite element method was applied to analyze and calibrate the chassis frame statically. First, the designed frame was modeled in 3D using CREO software and imported into ANSYS Workbench for meshing as shown in Figure 8. Among them, hexahedral and degenerate tetrahedral meshing is mainly used, with 703,281 nodes and 119,577 body cells.



**Figure 8.** Frame model meshing.

The constraints and the initial conditions of the force load are added on the basis of the frame mesh model, in which the spring loaded mass of the whole vehicle, i.e., the basic load of the frame, is shown in Table 3.

Table 3. Frame base load.

Part Name	Quantity	Full Load Weight/kg	Net Weight/kg	Load-Bearing Area/mm
Cab Assembly	1	500	500	9600
Engine Assembly	1	800	800	158,400
Medicine box assembly	1	4050	50	434,954
Fuel tank assembly	2	330	30	
Wash tank assembly	1	170	20	
Hydraulic oil tank assembly	1	85	10	25,200
Sparkling tank assembly	1	125	15	
Spray bar assembly	1	1100	1100	88,000
Mean score quality	-	250	250	737,200
Frame body assembly	-	1350	1350	-

### 3. Results and Discussion

#### 3.1. Frame Static Analysis Results

For different working conditions, the input of initial conditions is different. For the sprayer, four typical working conditions are analyzed, including bending, torsion, emergency braking and emergency turning. Bending condition refers to the spraying machine full load when the spray bar is unfolded in the working condition, when the spray bar is unfolded, the center of gravity of the spray bar is far from the main body of the frame to form a large bending moment; twisting condition for the spraying machine’s full load, one side of the wheel overhang caused the frame to twist; emergency braking refers to the spraying machine full load, the state when braking at maximum deceleration; emergency turning refers to the spraying machine full load, at a certain speed along the minimum turning radius when turning. The state of the sprayers. The stress and strain distributions of the frame are shown in Figure 9 by simulation calculations according to the constraints and loads added under different working conditions.

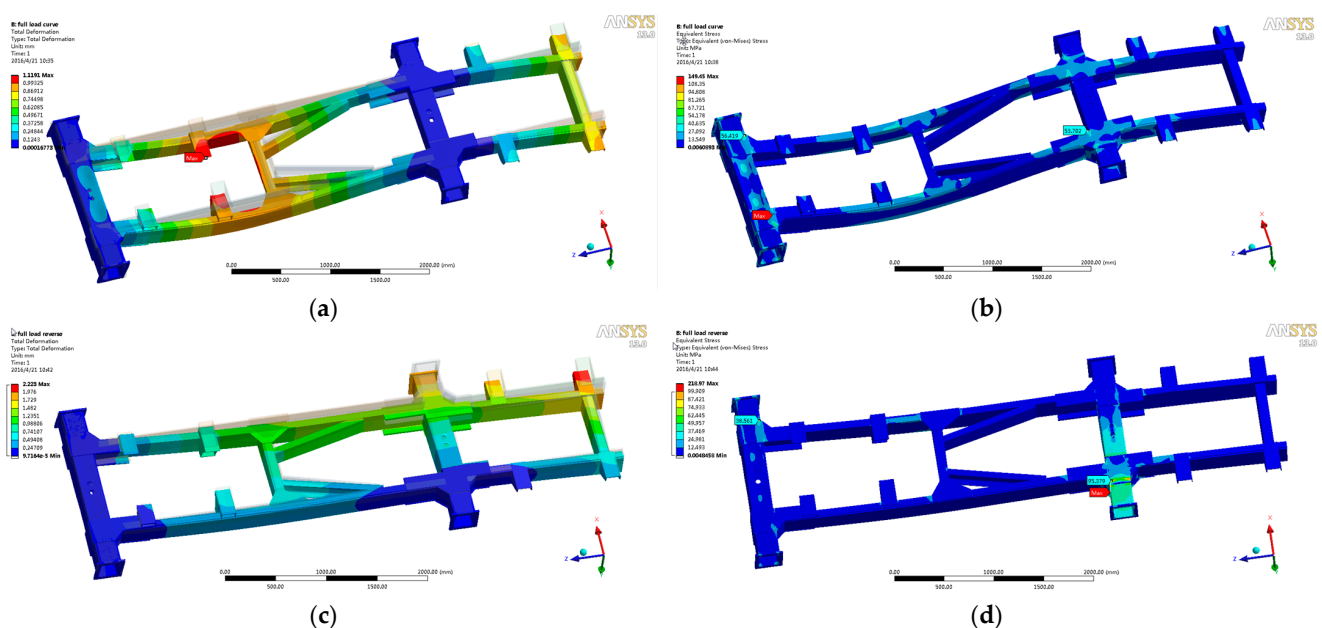
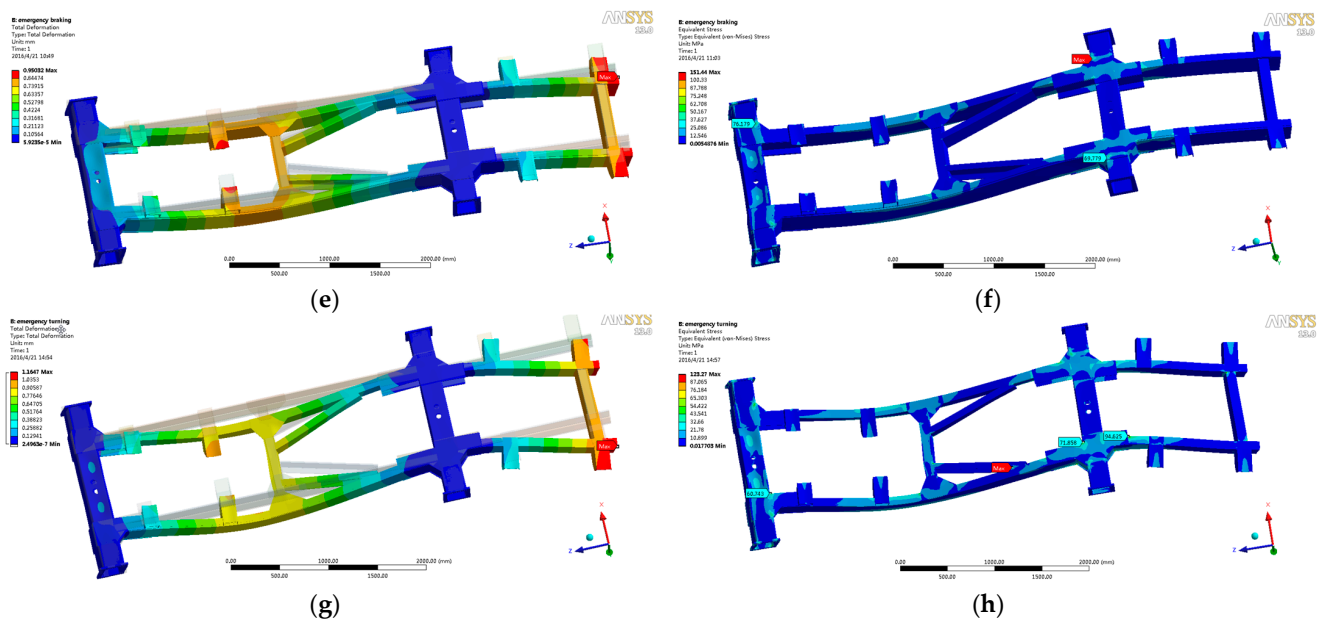


Figure 9. Cont.



**Figure 9.** Finite element analysis results of the frame for each working condition. (a) Frame strain distribution in bending conditions; (b) Bending condition frame stress distribution diagram; (c) Frame strain distribution for torsional conditions; (d) Torsional conditions frame stress distribution diagram; (e) Emergency braking conditions frame strain distribution; (f) Emergency braking condition frame stress distribution diagram; (g) Frame strain distribution for emergency turning conditions; (h) Frame stress distribution in emergency turning conditions.

From Figure 9a,b, it can be seen that the maximum deformation under bending conditions appears in the middle of the frame, the connection between the pillbox and engine mounting and the front end of the frame, with a deformation of 1.12 mm. The deformation caused to the front end of the frame is mainly due to the cab load on the front longitudinal beam equivalent to loading on a single cantilever beam, while the middle of the frame is mainly due to the collapse in the middle caused by the larger load. The calculated maximum stress value of 149.45 MPa occurs where the upper surface inside the axle housing is in contact with the inner side of the wheelbase adjusting rectangular beam, i.e., there is a stress concentration phenomenon. The reason for this is due to the special axle structure form. In the tubular axle, the innermost contact point of the wheelbase adjusting the rectangular beam with the axle shell will be caused by the sudden change of stress due to the abrupt change of the support point. The maximum stress in other parts is 56 Mpa, and the safety factor is high. From Figure 9c,d, it can be seen that the frame strain under torsional conditions performs well, with the maximum deformation of 2.22 mm, which appears at the left front end of the frame and the collapse of the left lower part of the cab. The maximum stress point is still at the edge of the front axle housing in contact with the wheelbase adjusting rectangular beam at 219 MPa. The overhang of the left front wheel exposes the frame to a large bending moment, and because the wheelbase adjusting rectangular beam is inserted in the axle housing, the section of the axle housing in contact with it cannot produce large and uniform deformation, so the stress concentration occurs at the edge of the contact. The maximum stress in the other parts without stress concentration is about 90 MPa. From Figure 9e,f, it can be seen that the overall deformation of the frame under the emergency braking condition is smaller, and the maximum stress is 151.44 MPa, which also appears in the stress concentration area described in the previous section. From Figure 9g,h, it can be seen that the frame still maintains good stiffness under the emergency turning condition, and the maximum stress point appears at the place where the strengthening beam is connected with the longitudinal beam at 123.27 MPa, which is due to the large transverse load on the frame, and the stress concentration appears at the narrow connection, while the stress concentration still appears at the contact section



between the crossbeam and the wheelbase adjustment rectangular beam, and the stress reaches 115 MPa. The stresses in other parts are generally found in the part where the crossmember is connected to the longitudinal beam, which is caused by the composite load consisting of transverse load and longitudinal load, with a maximum of 95 MPa.

According to the analysis results of each working condition, it is found that the overall rigidity of the frame is relatively good. Combined with the current frame design given by the truck frame deformation of not more than 10 mm standard, similar agricultural machinery standards specify the maximum static deflection of machinery does not exceed the maximum span of 0.5% of the standard, etc., the rigidity of the frame is fully acceptable and has a large optimization space. The strength safety factor is used to evaluate the static strength of the frame, and the expression is

$$n = \frac{\sigma_s}{\sigma_{\max}} \quad (12)$$

where  $\sigma_s$  is the material yield strength,  $\sigma_{\max}$  is the maximum equivalent force. The calculation results are shown in Table 4.

**Table 4.** Frame static strength evaluation results.

Typical Working Conditions	Dynamic Load Factor	Maximum Stress/MPa	Yield Strength/MPa	Safety Factor
Bend	2.5	149.45	345	2.3
Turning	1	218.97	345	1.6
Emergency Braking	2	151.44	345	2.3
Emergency Turns	2	123.27	345	2.8

According to the results in Table 4, the safety factor meets the requirements but there is no sufficient margin. From the results of stress calculation under each working condition, the maximum stress basically appears at the stress concentration, the overall stress level of the frame varies greatly, and the stress unevenness is obvious. According to the maximum stress at the non-stress concentration, the safety coefficients of the four working conditions are 6.1, 3.6, 4.5 and 3.6, respectively, so there will be a lot of room for optimization after solving the problem of stress concentration. Accordingly, the following optimization ideas are proposed:

1. To avoid stress concentration at the connection between the frame crossmember and the longitudinal beam and at the contact end between the axle housing and the wheelbase adjusting the rectangular beam by adopting measures such as smooth connection, increasing the rounded corners, changing the material of the axle housing and adding reinforcement bars;
2. Optimization of the location and form of the arrangement of crossbeams and strengthening beams to maximize the effectiveness of the materials;
3. Optimization of the cross-section of the longitudinal beam or reinforcement beam to achieve a more uniform stress level and to achieve a light weight.

### 3.2. Crossbeam and Reinforcement Beam Optimization Results

The optimization of the crossbeam and reinforcement beam positions of the frame is achieved by topology optimization to find the best distribution of materials. The topology optimization mesh model is divided in ANSYS Workbench as shown in Figure 10.

According to the static analysis of the frame, it can be seen that the deformation of the crossbeam mainly occurs in the bending condition. In addition, the local deformation in the torsional condition is larger and the working condition is more dangerous. Therefore, the optimization of the crossbeam and reinforcement beam position will be based on the bending condition and supplemented by the torsional condition. According to Table 3, frame load parameters are set to the boundary conditions, the initial value of topology

optimization to reduce the material is set to 80% and the optimization method is selected as multiple iterations performed automatically.

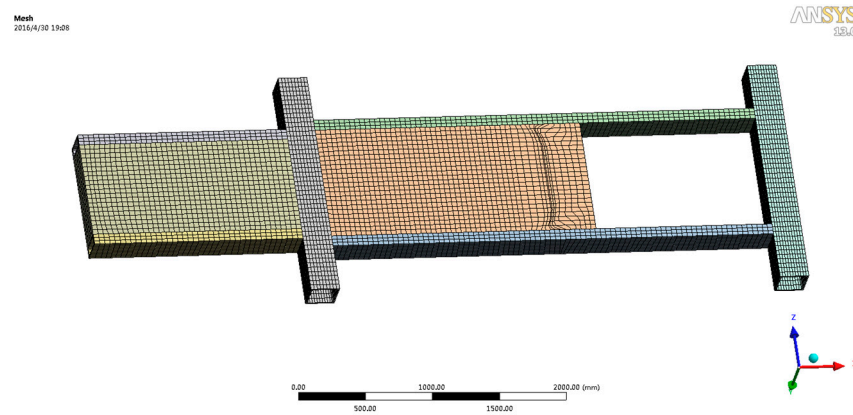


Figure 10. Topology-optimized finite element model.

The topology optimization results obtained when setting the percentage of material removed to 82% under the bending condition are shown in Figure 11.

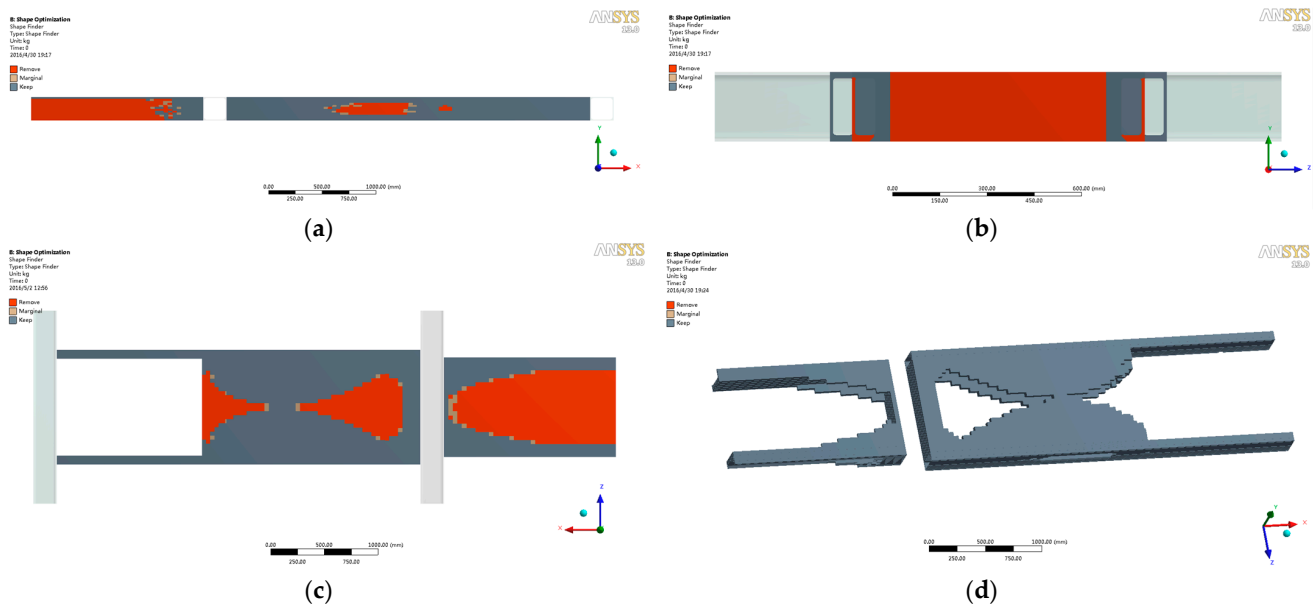
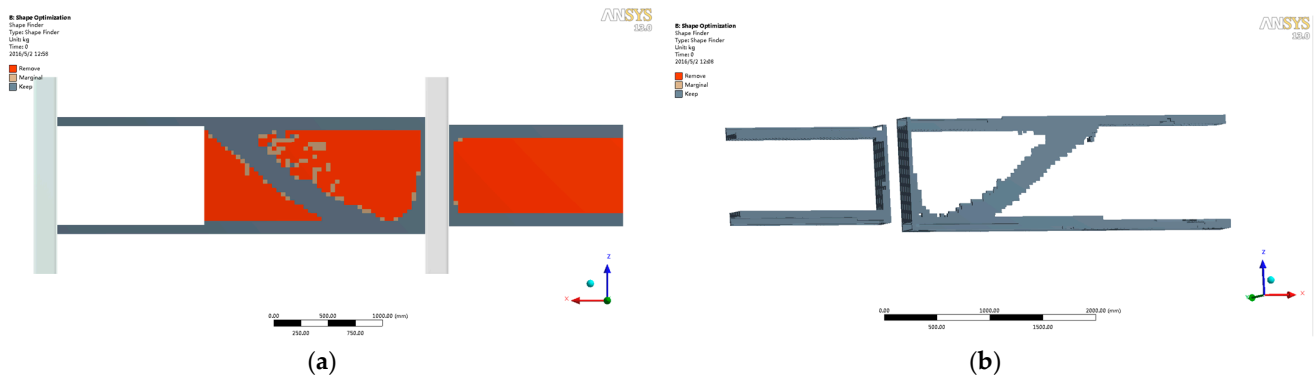


Figure 11. Topology optimization results for static bending conditions. (a) Front face; (b) Left face; (c) Top face; (d) Retained fraction with density of 1.

As can be seen from Figure 11, the optimization results suggest leaving the rear longitudinal beam because most of its position has to bear the load, but Figure 11a,b show that the stacked front longitudinal beam is considered to have a low contribution to the overall vehicle stiffness in the optimization process and is suggested to be changed to a slotted cross-section longitudinal beam, taking into account that because the front longitudinal beam is a cantilever beam, the stress generated by bearing the cab load needs to be considered, so the stacked longitudinal beam is retained, but the longitudinal beam size needs to be optimized for weight reduction. The front crossmember is considered to have little effect on the overall frame stiffness, but because some of its functional effects cannot be completely removed, it can be changed into a slotted beam and reduce the thickness. Figure 11c,d diagrams show that the position of the middle crossmember is recommended to be moved forward, and the form of the reinforcement beam is changed from half X form to full X form. The reinforcement beam immediately adjacent to the

longitudinal beam is recommended to be triangularly connected with the longitudinal beam and crossmember. The b diagram shows that the outer side of the rear longitudinal beam is also recommended to be partially hollowed out. Considering the manufacturing process and economic efficiency, the complete longitudinal beam will be retained, but the size of the rear longitudinal beam also needs to be optimized to achieve weight reduction.

The torsional condition is used as an auxiliary analysis condition, mainly looking at the unit part with the highest contribution to the stiffness, so the removal material percentage is set to 90% and the topology optimization structure of the torsional condition is obtained as shown in Figure 12.



**Figure 12.** Topology optimization results for torsional conditions. (a) Top face; (b) Retained fraction with density of 1.

The optimization results show that in the torsional condition, the unit with the highest contribution to the overall frame stiffness is mainly the shape of the inclined crossmember distributed in the middle of the frame. At this time, it is the twisting case formed by the removal of the support of the left front wheel. Due to the symmetry of the whole vehicle load and frame shape, it is easy to think of the twisting case of the removal of the support of the right front wheel, and it is obtained that in the twisting condition, the unit with the highest contribution to the frame stiffness is mainly located in the middle of the frame, and the overall X shape, which is consistent with the optimization results of the bending condition.

Combining the above optimization results, the optimized overall frame scheme is obtained as shown in Figure 13. In the figure, 3 is the forward-moving crossbeam and 4 and 9 are the reinforcement beams in an X-shape after optimization.

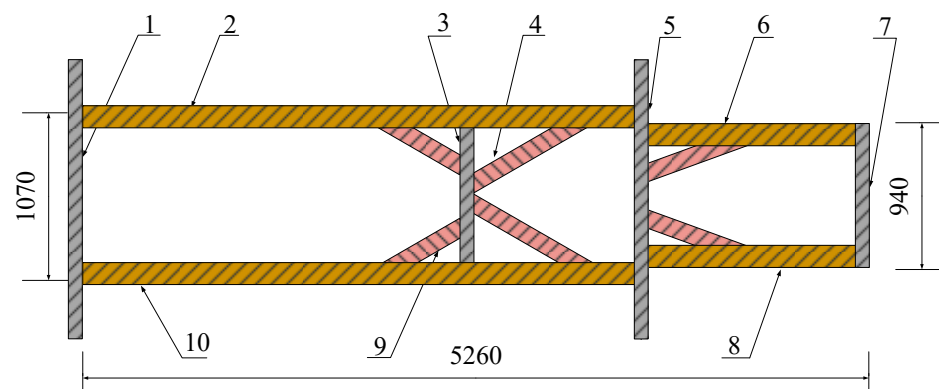


**Figure 13.** Overall scheme of optimized frame structure.

The optimized frame structure was analyzed statically again, and the results are shown in Figure 14. According to the comparison between the results of finite element analysis

after frame optimization and before optimization, the performance changes are shown in Table 5.

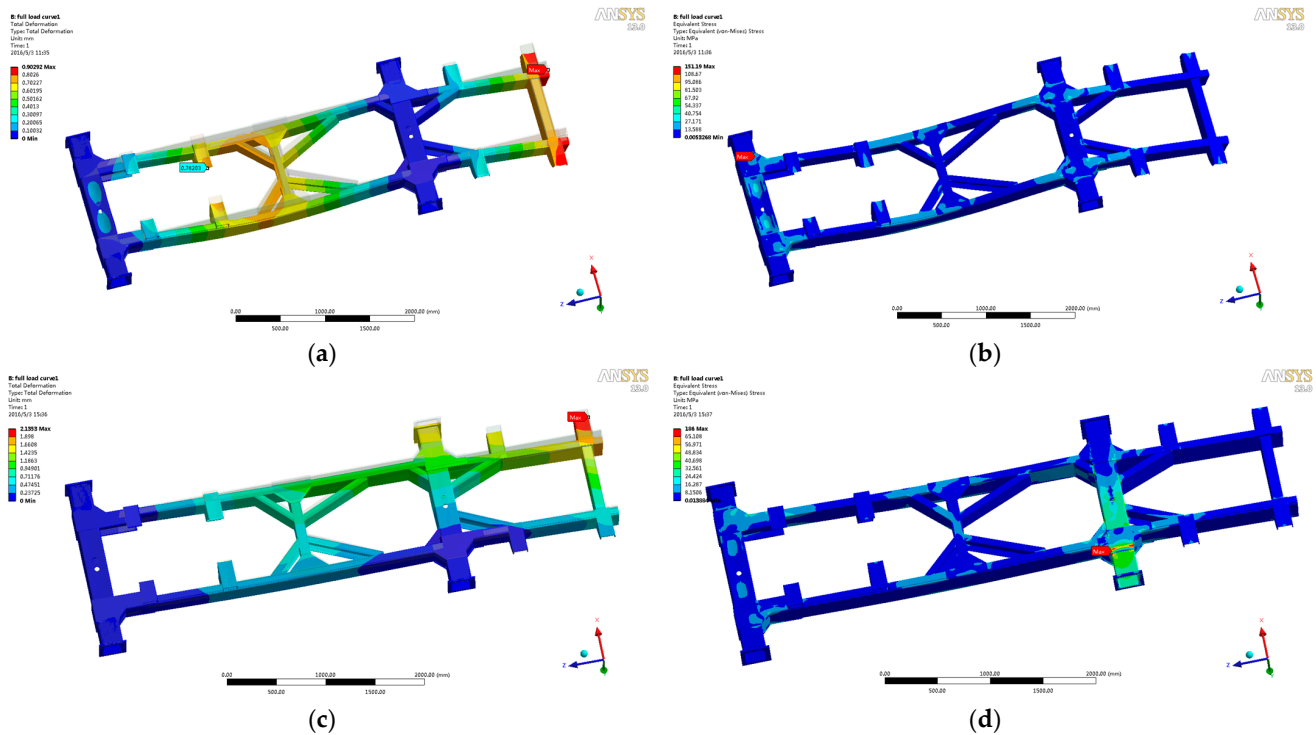


**Figure 14.** Finite element analysis results of frame optimization structure. (a) Frame strain distribution in bending conditions; (b) Bending condition frame stress distribution diagram; (c) Frame strain distribution for torsional conditions; (d) Torsional conditions frame stress distribution diagram.

**Table 5.** Initial values of optimization variables and optimization results.

Optimization Variables	Before Optimization	After Optimization	Range of Change
Frame Quality	1117.3 kg	1092.3 kg	−2.2%
Maximum Deformation in Bending Condition	1.12 mm	0.90 mm	−19.4%
Maximum Stress in Bending Condition	149.45 MPa	151.40 MPa	+1.1%
Maximum Deformation in Torsional Conditions	2.22 mm	2.13 mm	−4.1%
Maximum Stress in Torsional Conditions	219 MPa	186 MPa	−15.1%

From Table 5, it is clear that the topology optimization with frame deformation as the optimization target has a certain optimization effect. With no increase in the overall frame material, the bending resistance and torsional resistance of the frame have been improved, especially in the middle of the frame at the location of the optimized crossbeam and reinforcement beam, the stiffness has increased significantly.

### 3.3. Longitudinal Beam Optimization Results

The analysis of the static results of the frame shows that the overall stress level is relatively uneven, especially the stress level of the front and rear longitudinal beams is much lower than the average stress level; therefore, the cross-sectional dimensions of the front and rear longitudinal beams need to be optimized. The cross-section of the longitudinal beam is shown in Figure 4c, and only the overall width  $b$  and thickness  $t$  of the longitudinal beam are optimized because its height  $h$  is related to the axle. The multi-objective driven optimization design is carried out by the Design Exploration module in Workbench, with the width and thickness of the longitudinal beam as input parameters named DS\_WIDTH and DS\_THICKNESS. The constraint loads under bending and torsional conditions are

applied, with the overall frame Geometry Mass, the Equivalent Stress Maximum and Total Deformation Maximum as output parameters. In the GDO module, the width range was set from 60 to 72 mm and the thickness from 6 to 11 mm, the maximum deflection of the frame was set to 1 mm, the maximum torsional deformation to 2 mm and the maximum stress to 156 MPa. The local sensitivity histograms and response surfaces of the input and output parameters are shown in Figures 15 and 16.

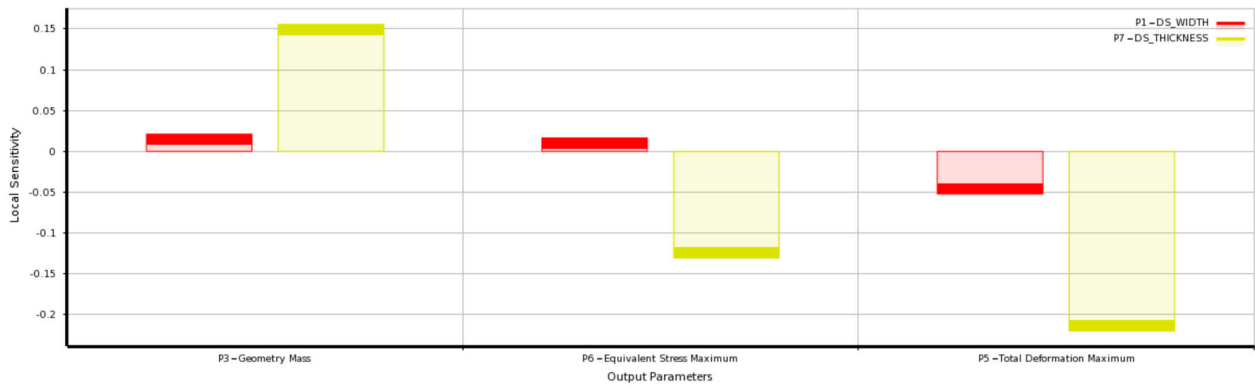


Figure 15. Histogram of local sensitivity of input parameters to output parameters.

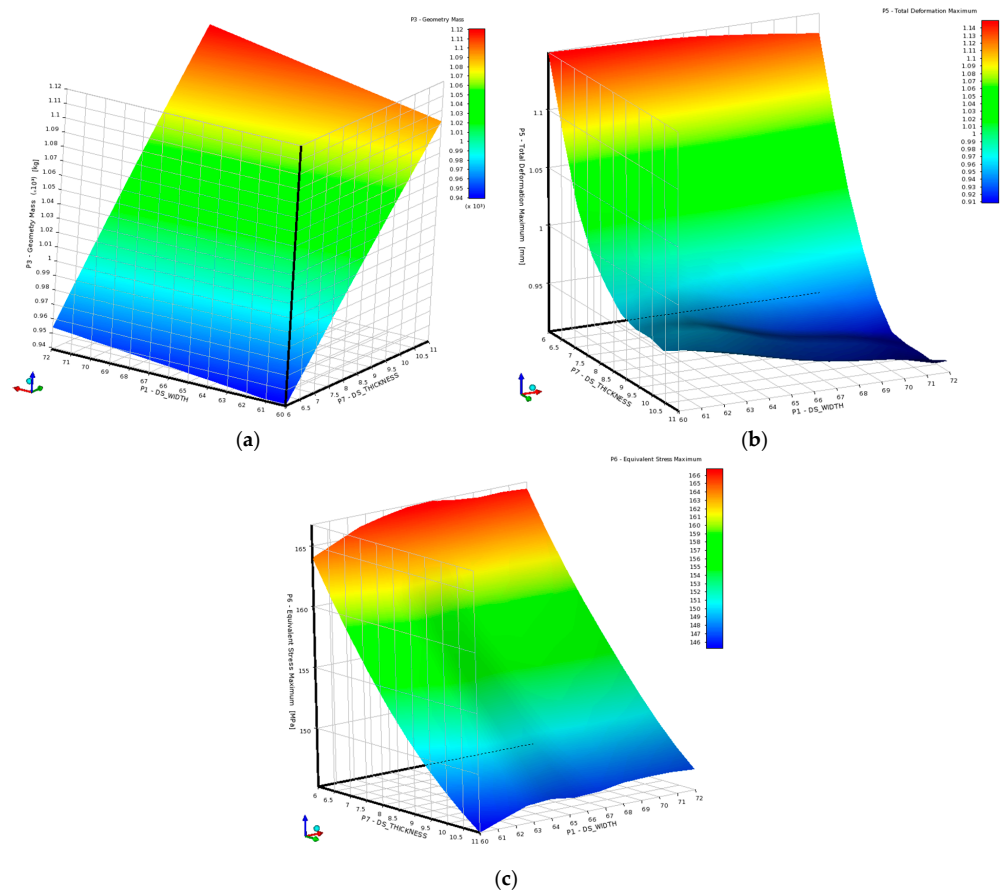


Figure 16. Response surface of structural parameters and objective function. (a) Effect of cross-sectional width and thickness of longitudinal beam on frame quality; (b) Influence of the width and thickness of the longitudinal beam section on the maximum deformation of the frame; (c) Effect of section width and thickness of longitudinal beam on the maximum stress in the frame.

An analysis of Figures 15 and 16 shows that the thickness of the longitudinal beam is what affects the strength and stiffness more in the longitudinal beam cross-section. The

response surface is an approximate surface consisting of the basic design points, which is very close to the real response surface obtained by the method of sample interpolation iteration. In the subsequent selection, the optimal design points will be selected by the response surface, and then the parameters of the optimal design points will be brought back to the analysis program to obtain the final optimal results.

Based on the above results and constraints, the three optimal parameter combinations for the two operating conditions are calculated as shown in Figure 17.

	P1 - DS_WIDTH	P7 - DS_THICKNESS	P3 - Geometry Mass (kg)	P6 - Equivalent Stress Maximum (MPa)	P5 - Total Deformation Maximum (mm)
Optimization Study					
Objective	No Objective	No Objective	Values <= Target	Values <= Target	Values <= Target
Target Value			1050	156	1
Importance	Default	Default	Default	Default	Default
Candidate Points					
Candidate A	← 66.555	← 8.0834	★ 1015.9	← 155.73	★ 0.9579
Candidate B	← 60.002	← 8.5003	★ 1017.5	★ 152.4	★ 0.96943
Candidate C	← 62.795	← 8.98	← 1037.5	★ 153.12	★★ 0.95169

(a)

	P1 - DS_WIDTH	P7 - DS_THICKNESS	P3 - Geometry Mass (kg)	P6 - Equivalent Stress Maximum (MPa)	P5 - Total Deformation Maximum (mm)
Optimization Study					
Objective	No Objective	No Objective	Values <= Target	Values <= Target	Values <= Target
Target Value			1050	156	2
Importance	Default	Default	Default	Default	Default
Candidate Points					
Candidate A	← 63.679	← 9.1216	← 1043.5	★★ 150.61	★ 1.992
Candidate B	← 60.002	← 8.5003	★ 1017.5	← 155.83	★ 1.9951
Candidate C	← 61.336	← 9.0105	← 1035.6	★ 153.71	★ 1.9887

(b)

**Figure 17.** Optimal results for three sets of parameters at each working condition. (a) Bending conditions; (b) Torsional working conditions. The gray short line in the figure indicates that the optimization result is average, while the star mark indicates that the optimization effect is good. The more stars, the better the optimization result.

From Figure 17a,b, it can be seen that the combination of frame parameters Candidate B is optimal in both operating conditions; therefore,  $b = 60$  and  $t = 8.5$  are formulated as the optimal parameters of the frame, and static comparative analysis is carried out under these parameters to obtain the final optimized strain and equivalent force results of the frame as shown in Figure 18. The change rates of each evaluation index after comparison and optimization are shown in Table 6.

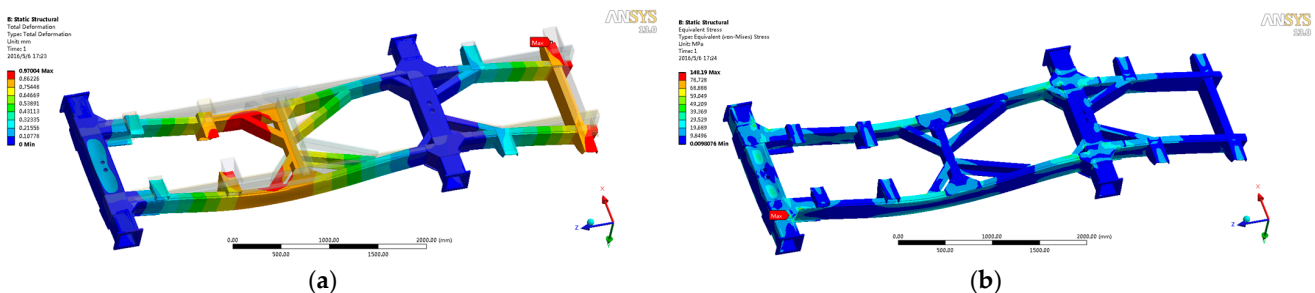


**Figure 18.** Results of static analysis of bending conditions after optimization. (a) Strain distribution map; (b) Stress distribution map.



**Table 6.** Initial values of optimization variables and optimization results.

Optimization Variables	Before Optimization	After Optimization	Range of Change
Width of Longitudinal Beam $b$	70 mm	60 mm	−14.3%
Thickness of Longitudinal Beam $t$	10 mm	8.5 mm	−15%
Total Frame Mass	1092.3 Kg	1017.5 Kg	−6.8%
Maximum Deformation	0.903 mm	0.970 mm	+7.4%
Maximum Stress	151.10 MPa	148.2 MPa	−1.9%

As can be seen from Table 6, although the maximum frame deformation increases by 7.4%, the value remains within the target range and can meet the basic requirements of frame strain. The maximum stress is slightly reduced and the total frame mass is reduced by 6.8%; correspondingly, the rear longitudinal beam of the frame is reduced by 18.9%, which achieves the purpose of local lightweighting. Meanwhile, the analysis results in Figure 18 show that the stress level of the rear longitudinal beam of the frame has increased and the local stress level is more uniform. This result indicates that the optimized longitudinal beam section has better mechanical properties and is more in line with the theoretical value of optimal bending resistance.

#### 4. Conclusions

High ground clearance self-propelled sprayer is an important machine for agricultural application, and improving its performance is an effective means to improve the application technology. In this paper, a new structure of sprayer frame is designed for one of the important components of sprayer, and the frame structure and important parameters are optimized by means of static analysis and optimization design theory to improve its stiffness and strength while achieving the purpose of lightweight frame. The specific conclusions are as follows:

1. According to the structure and operating characteristics of the sprayer, the overall arrangement of the vehicle was determined as a rear-mounted spray bar and a mid-mounted engine, based on which a disconnected longitudinal beam frame with an X-shaped reinforcement beam, was determined. The crossbeam and longitudinal beam, which are important parts of the frame, were designed, and the crossbeam cross-section size and the working principle of wheelbase adjustment were initially determined.
2. According to the characteristics of the load on the frame of the sprayer during operation, the static analysis of the chassis frame under four typical working conditions, such as bending, torsion, emergency braking and emergency turning, was carried out using the finite element method. The maximum frame deformation is 2.22 mm and the maximum stress is 219 MPa.
3. The topology optimization method was applied to optimize the crossbeam and reinforcement beam positions, resulting in a 2.2% reduction in overall frame mass, a 19.4% reduction in maximum deformation while maintaining a small change in maximum stress under bending conditions and a 4.1% and 15.1% reduction in maximum deformation and maximum stress, respectively, under torsional conditions. The frame-section width and thickness parameters were optimized by multi-objective driven optimization. The results showed that the frame mass and maximum stress were reduced by 6.8% and 1.9%, respectively, in the bending condition at the cost of a slight increase in frame deformation.

The research results of this paper can provide a digital design and optimization idea for the research related to the chassis frame of large upland gap self-propelled sprayer to improve the driving performance and spraying quality of the whole sprayer, which is of practical significance to further improve the application technology.

**Author Contributions:** Conceptualization, L.L. and B.L.; methodology, L.L. and B.L.; software, B.L.; validation, L.L. and B.L.; formal analysis, B.L.; investigation, L.L.; resources, Y.C.; data curation, B.L.; writing—original draft preparation, L.L.; writing—review and editing, L.L. and Y.C.; visualization, B.L.; supervision, E.M., Z.S. and J.C.; project administration, Y.C.; funding acquisition, Y.C. All authors have read and agreed to the published version of the manuscript.

**Funding:** This research was funded by the National Natural Science Foundation of China (32001428), the Key R&D projects in Shaanxi Province (2022NY-205) and the Shaanxi Provincial Key Industry Innovation Chain (Cluster) Project (2023-DLNY-62).

**Institutional Review Board Statement:** Not applicable.

**Data Availability Statement:** Not applicable.

**Conflicts of Interest:** The authors declare no conflict of interest.

## References

- Feng, Y.N.; Pei, L.; Chen, X.; Chen, X.B.; Liu, Y.; Chen, B. Summary of the key technology of variable rate application. *J. Chin. Agric. Mech.* **2021**, *42*, 65–71. [[CrossRef](#)]
- Hu, Y.H.; Yang, H.B.; Hou, B.R.; Xi, Z.T.; Yang, Z.D. Influence of Spray Control Parameters on the Performance of an Air-Blast Sprayer. *Agriculture* **2022**, *12*, 1260. [[CrossRef](#)]
- Wang, H.Y. Research on the current situation and development trend of agricultural plant protection machinery technology application. *Farm Staff* **2019**, *10*, 119–120.
- Wang, X.M. Agricultural plant protection machinery technology application status and development trend. *Use Maint. Agric. Mach.* **2019**, *03*, 74–75. [[CrossRef](#)]
- Li, S.F. Structure Simulation and Optimization of Largestraddle-Row Self-Propelled Orchard Sprayer Based on Multi-Body Dynamics. Master's Thesis, Jiangu University, Zhenjiang, China, 2021.
- Chen, Y. Research on Design Methods and Characteristics of Independent Strut Type Air Suspension System for High Clearance Sprayer. Ph.D. Thesis, China Agricultural University, Beijing, China, 2017.
- Li, W.; Yang, F.; Mao, E.R.; Shao, M.X.; Sui, H.C.; Du, Y.F. Design and Verification of Crab Steering System for High Clearance Self-Propelled Sprayer. *Agriculture* **2022**, *12*, 1893. [[CrossRef](#)]
- Sartori, S.; Balthazar, J.M.; Pontes, B.R. Non-linear dynamics of a tower orchard sprayer based on an inverted pendulum model. *Biosyst. Eng.* **2009**, *103*, 417–426. [[CrossRef](#)]
- Wang, Z.H.; Wu, J.B.; Liu, J.W. Multi-Condition Analysis and Optimization of Sprayer Frame. *Appl. Mech. Mater.* **2016**, *835*, 632–638. [[CrossRef](#)]
- Kappaun, R.; Meira, A.D.D.; Walber, M. Parameters for modeling passive suspensions of spray bars. *Eng. Agric.* **2021**, *41*, 368–378. [[CrossRef](#)]
- Cui, L.F.; Xue, X.Y.; Le, F.X. Adaptive robust precision control of an active spray boom suspension with disturbance estimation. *J. Vib. Control* **2021**, *29*, 3–4. [[CrossRef](#)]
- Yu, Z.N. Design and Experimental Research on Spray Bar Suspension of High Clearance spray. Master's Thesis, Heilongjiang Bayi Agricultural University, Daqing, China, 2021.
- Cui, L.F.; Xue, X.Y.; Le, F.X.; Mao, H.P.; Ding, S.M. Design and experiment of electro hydraulic active suspension for controlling the rolling motion of spray boom. *Int. J. Agric. Biol. Eng.* **2019**, *12*, 72–81. [[CrossRef](#)]
- Han, J.H.; Park, C.H.; Jang, Y.Y.; Gu, J.D.; Kim, C.Y. Performance Evaluation of an Autonomously Driven Agricultural Vehicle in an Orchard Environment. *Sensors* **2022**, *22*, 114. [[CrossRef](#)] [[PubMed](#)]
- Wang, S.B.; Song, J.L.; Qi, P.; Yuan, C.J.; Wu, H.C.; Zhang, L.T.; Liu, W.H.; Liu, Y.J.; He, X.K. Design and development of orchard autonomous navigation spray system. *Front. Plant Sci.* **2022**, *13*, 960686. [[CrossRef](#)] [[PubMed](#)]
- Wang, G.Q.; Feng, J.A.; Yu, X.S.; Song, B. Optimization of operation ride comfort for locomotive-liquid-road coupling of high-clearance sprayer. *J. Vib. Shock* **2021**, *40*, 140–150. [[CrossRef](#)]
- Gonzalez-de-Soto, M.; Emmi, L.; Perez-Ruiz, M.; Aguera, J.; Gonzalez-de-Santos, P. Autonomous systems for precise spraying—Evaluation of a robotised patch sprayer. *Biosyst. Eng.* **2016**, *146*, 165–182. [[CrossRef](#)]
- Liu, H.; Long, Y.N.; He, S.W.; Cui, Y.M.; Sheng, Y. Design and experiment of the auxiliary steering system for a four-wheel independent electrically driven high clearance sprayer. *Trans. Chin. Soc. Agric. Eng.* **2021**, *37*, 30–37. [[CrossRef](#)]
- Zhou, Q.Q.; Wen, H.J.; Li, Z.X.; Zhang, W.R.; Yi, Z.T.; Wang, G.T. Design and Test of Fuzzy Anti-skid Control of Four-wheel Drive Hydraulically Driven Sprayer. *Trans. Chin. Soc. Agric. Mach.* **2020**, *51*, 283–288. [[CrossRef](#)]
- Pontelli, C.O.; Mucheroni, M.F.; Balthazar, J.M.; Pontes, B.R. Comparison between two types of passive boom suspension under simulated conditions of track test. *Eng. Agric.* **2010**, *30*, 761–775. [[CrossRef](#)]
- Xue, X.B. Finite Element Analysis and Structural Optimization of Fence Spray Frame with Single Front Wheel Steering and Single Rear Wheel Drive. Master's Thesis, Yangzhou University, Yangzhou, China, 2011.
- Chen, Y.; Mao, E.R.; Li, W.; Zhang, S.; Song, Z.H.; Yang, S.J.; Chen, J. Design and experiment of a high-clearance self-propelled sprayer chassis. *Int. J. Agric. Biol. Eng.* **2020**, *13*, 71–80. [[CrossRef](#)]

23. Wu, B. Finite Element Analysis and Lightweight Research on Hydraulic Chassis Frame of Self-Propelled Paddy Field Boom Sprayer. Master's Thesis, Jiangsu University, Zhenjiang, China, 2021.
24. Chen, H.; Dai, S.; Ou, M.; Li, S.; Wang, C.; Li, Z.; Wang, G.; Chen, Y.; Jia, W. Multibody Dynamics Simulation and Vibration Test for High Clearance Orchard Sprayer. *Appl. Sci.* **2022**, *12*, 8058. [[CrossRef](#)]
25. Zheng, X. Finite Element Analysis and Optimization Design of Bus Frame Structure. Master's Thesis, Dalian University of Technology, Dalian, China, 2004.
26. Liang, J.B.; Lv, J.C. Topological Optimization Design of Engine Support Based on HyperWorks. *Heavy Truck* **2009**, *03*, 16–17.
27. Long, K.; Tan, W.J.; Zuo, Z.X. Optimization design of tractor frame based on topological optimization method. *J. Mach. Des.* **2007**, *6*, 52–54. [[CrossRef](#)]
28. Zhao, C.Z.; Zhang, C.L.; Li, Y.; Bo, C.Z.; Hao, G.F.; Dou, H.B. Design and optimization of the frame of the air-driven electrostatic spray locomotive. *J. Phys. Conf. Ser.* **2020**, *1650*, 022057. [[CrossRef](#)]
29. Han, H.Y.; Chen, S.Y.; Shao, J.S.; Yao, Y.; Chen, G. Lightweight design of chassis frame for motor boom sprayer. *Trans. Chin. Soc. Agric. Eng.* **2013**, *29*, 47–53. [[CrossRef](#)]
30. Wang, X.F. *Automotive Chassis Design*; Tsinghua University Press: Beijing, China, 2010; pp. 4–5.

**Disclaimer/Publisher's Note:** The statements, opinions and data contained in all publications are solely those of the individual author(s) and contributor(s) and not of MDPI and/or the editor(s). MDPI and/or the editor(s) disclaim responsibility for any injury to people or property resulting from any ideas, methods, instructions or products referred to in the content.